Title

Sost and its paralog Sostdc1 coordinate digit number in a Gli3-dependent manner.

Journal

Developmental biology, 383(1)

ISSN

0012-1606

Authors

Collette, Nicole M
Yee, Cristal S
Murugesh, Deepa
et al.

Publication Date

2013-11-01

DOI

10.1016/j.ydbio.2013.08.015

Peer reviewed

HHS Public Access

Author manuscript

Dev Biol. Author manuscript; available in PMC 2013 December 12.

Published in final edited form as:

Dev Biol. 2013 November 1; 383(1): 90–105. doi:10.1016/j.ydbio.2013.08.015.

Sost and its paralog *Sostdc1* coordinate digit number in a Gli3-dependent manner☆

Nicole M. Collette[a], **Cristal S. Yee**[a,b], **Deepa Murugesh**[a], **Aimy Sebastian**[a,b], **Leila Taher**[c,d], **Nicholas W. Gale**[e], **Aris N. Economides**[e], **Richard M. Harland**[f], and **Gabriela G. Loots**[a,b,*]

Gabriela G. Loots: loots1@llnl.gov, ggloots@gmail.com

[a]Biology and Biotechnology Division, Lawrence Livermore National Laboratory, 7000 East Avenue, L-452, Livermore, CA 94550, USA

[b]School of Natural Sciences, University of California, Merced, CA, USA

[c]Computational Biology Branch, National Center for Biotechnology Information, National Library of Medicine, National Institutes of Health, Bethesda, MD, USA

[d]Institute for Biostatistics and Informatics in Medicine and Ageing Research, University of Rostock, Rostock, Germany

[e]Regeneron Pharmaceuticals, Tarrytown, NY, USA

[f]Molecular and Cell Biology Department, University of California, Berkeley, CA, USA

Abstract

WNT signaling is critical in most aspects of skeletal development and homeostasis, and antagonists of WNT signaling are emerging as key regulatory proteins with great promise as therapeutic agents for bone disorders. Here we show that *Sost* and its paralog *Sostdc1* emerged through ancestral genome duplication and their expression patterns have diverged to delineate non-overlapping domains in most organ systems including musculoskeletal, cardiovascular, nervous, digestive, reproductive and respiratory. In the developing limb, *Sost* and *Sostdc1* display dynamic expression patterns with *Sost* being restricted to the distal ectoderm and *Sostdc1* to the proximal ectoderm and the mesenchyme. While *Sostdc1*$^{-/-}$ mice lack any obvious limb or skeletal defects, *Sost*$^{-/-}$ mice recapitulate the hand defects described for Sclerosteosis patients. However, elevated WNT signaling in *Sost*$^{-/-}$; *Sostdc1*$^{-/-}$ mice causes misregulation of SHH signaling, ectopic activation of *Sox9* in the digit 1 field and preaxial polydactyly in a Gli1- and Gli3-dependent manner. In addition, we show that the syndactyly documented in Sclerosteosis is present in both *Sost*$^{-/-}$ and *Sost*$^{-/-}$; *Sostdc1*$^{-/-}$ mice, and is driven by misregulation of *Fgf8* in the AER, a region lacking *Sost* and *Sostdc1* expression. This study highlights the complexity of WNT signaling in

*Corresponding author at: Biology and Biotechnology Division, Lawrence Livermore National Laboratory, 7000 East Avenue, L-452, Livermore, CA 94550, USA.

Appendix A. Supporting information: Supplementary data associated with this article can be found in the online version at http://dx.doi.org/10.1016/j.ydbio.2013.08.015.

skeletal biology and disease and emphasizes how redundant mechanism and non-cell autonomous effects can synergize to unveil new intricate phenotypes caused by elevated WNT signaling.

Keywords

WNT signaling; *Sost*; Sclerostin; *Sostdc1*; Shh; Limb formation; Polydactyly; syndactyly

Introduction

Gene duplication is at the center of evolutionary diversification and represents a dominant contributor to biological innovation. The process of gene duplication is the main mechanism by which paralogous genes with redundant functions emerge, and represents a means of protecting an organism against deleterious mutations (Hoffmann et al., 2010; Moleirinho et al., 2011). At the same time, genes that are not critical (where a critical gene is described by a lethal embryonic phenotype) are more likely to evolve under less stringent selective pressure, and in the case of duplicated genes, maintain some partial functional redundancy. The gene encoding Sclerostin or *Sost* is located on human chromosome 17 and its protein sequence was found to be 55% similar to a homologous gene, *Sostdc1*, located on chromosome 7 (Fig. 1). In humans and mouse models *Sost* deficiency causes Sclerosteosis, a rare autosomal recessive disorder, characterized by generalized hyperostosis of the axial and appendicular skeleton (Balemans et al., 2001; Collette et al., 2012). Due to its highly specialized null phenotype, and abundant transcription in bone, primarily osteocyte-derived, sclerostin was originally described as a protein exclusively secreted by osteocytes that functions as a negative regulator of bone formation (van Bezooijen et al., 2005; Winkler et al., 2003), through antagonizing the BMP signaling pathway; later was found to also bind to LRP5/6 co-receptors and antagonize WNT signaling (Kusu et al., 2003; Li et al., 2005; Semenov et al., 2005; ten Dijke et al., 2008; van Bezooijen et al., 2007b; Winkler et al., 2003).

Similar to *Sost*, its paralog *Sostdc1* (Sost domain-containing protein 1; aka *Sostl*, *USAG-1*, *Wise*, *ectodin*) has been described as a WNT antagonist (Ahn et al., 2010), as well as an inhibitor of BMP signaling (Lintern et al., 2009; Murashima-Suginami et al., 2008). *SOSTDC1* has been shown to be expressed in the kidney (Blish et al., 2010; Turk et al., 2009), lung (Zhang et al., 2012), the developing tooth bud of ferrets (Jarvinen et al., 2009), and SNPs in *SOSTDC1* have been associated with a low bone-mass phenotype in Chinese women, consistent with a possible role in maintaining functions of the musculoskeletal system (He et al., 2011). *Sostdc1*-deficient mice display severe teeth defects characterized by enlarged enamel knots, altered cusp patterns, fused molars, and extra teeth (supernumerary incisors) (Kassai et al., 2005; Munne et al., 2009). In addition, *Sostdc1* has been shown to be highly expressed in distal convoluted tubules and connecting tubules in the kidney (Tanaka et al., 2008) and *Sostdc1*-deficient mice were shown to be resistant to tubular injury in an acute renal failure and interstitial fibrosis rodent model, revealing that *Sostdc1* may influence the progression of kidney disease (Yanagita et al., 2006). Although *Sost* and *Sostdc1* have been studied primarily from the perspectives of bone mass and kidney response to injury, respectively, here we show that these genes are broadly expressed in the

mouse during development and adulthood, and we dissect their shared roles during limb development.

We have recently shown that in addition to functioning as a WNT antagonist in the adult bone, *Sost* also plays a critical role as a negative regulator of WNT signaling in the developing limb. A less common human phenotype described for sclerosteosis patients is the occasional presence of hand defects at birth. These abnormalities are primarily characterized by syndactyly [asymmetric cutaneous or bony syndactyly of the index and middle fingers (digits 2 and 3)] and radial deviation of the digits, with hypoplasia and nail dysplasia (symmetric or asymmetric; most commonly associated with the index finger) (Hamersma et al., 2003; Itin et al., 2001; Sugiura and Yasuhara, 1975).

Moreover, using a genetic approach we have previously demonstrated that over-expression of human *SOST* from a bacterial artificial chromosome (BAC) perturbs anterior–posterior and proximal–distal patterning of the developing limb. These transgenic mice showed a wide range of limb defects including fused, split, missing bones and whole digits and the severity of the limb defects were shown to be dose-dependent. We also showed that *Sost*-deficiency rescued significant aspects of the *Lrp6*$^{-/-}$ skeletal phenotypes supporting the view that *SOST* gain-of-function impairs limb patterning by inhibiting WNT signaling through the LRP5/6 co-receptors (Collette et al., 2010).

Because of the evolutionary relationship between *Sost* and *Sostdc1* as well as their common molecular roles as WNT-, and possibly BMP- antagonists, we have examined the shared and unique functions of these paralogs, in single and double knockout mice. Initially, we describe in detail, both the embryonic and adult tissue distribution of these transcripts through the use of *LacZ*-knock-in alleles. We find both genes to have dynamic and complex expression patterns during embryonic and limb development, and are often expressed in adjacent tissues or cell types. In the adult mouse, we find *Sostdc1* to be more widely distributed than *Sost*; however significant expression of *Sost* was detected in non-skeletal tissues. In general, when these genes are expressed in the same organ system, they are present in non-overlapping expression domains, suggesting that these genes have evolved different sub-specializations within the signaling pathways they regulate, as a function of their cellular location.

In particular, we focused our analysis on the characterization of their shared roles during limb development. Herein, we show that *Sost* deficient mice recapitulate the hand defects described for sclerosteosis patients (Itin et al., 2001), at a frequency of 4%, while *Sostdc1*$^{-/-}$ lack any skeletal patterning defects; they do display mild ventralization characterized by pigmentation and hair growth on the ventral side of the autopod. We also find that consistent with their site of gene expression in the developing limb, *Sost*$^{-/-}$; *Sostdc1*$^{-/-}$ mice exhibit preaxial polydactyly, detected visually as early as E11.5, indicating that *Sost* and *Sostdc1* play partially redundant and complementary roles in the developing limb. Through a combination of *in situ* marker and micro-array gene expression analysis we show that the combined absence of *Sost* and *Sostdc1* interferes with components of WNT, BMP, SHH, FGF and TGFb signaling to produce several limb abnormalities that include: preaxial polydactyly, syndactyly, dorsalization, radial deviation and nail dysplasia. In particular we

show that the preaxial polydactyly is driven by misregulation of SHH signaling, where the *Shh* and *Gli1* expression domains are elevated and expanded anteriorly, while *Gli3* expression levels are reduced. *Grem1* expression is missing in the anterior mesenchyme of the limb bud where the duplicated digits form, and *Hoxd13* is ectopically expressed. We conclude that *Sox9* ectopic activation in the digit 1 field is promoted by the misexpression of *Gli1* transcription factor, which has been previously shown to control *Sox9* transcription, and by the lack of *Gli3*-dependent gene repression. We also examined the underlying causes of the observed syndactyly, and found *Fgf8* levels to be elevated, and BMP4 and BMP7 to be absent in the AER; the *Fgf8* AER expression domain is expanded proximally and disorganized which resulted in a reduction in interdigital apoptosis in regions corresponding to the observed syndactyly. Thus, the absence of *Sost* and *Sostdc1* in the limb disrupts the epithelial–mesenchymal communication required for proper limb patterning in these compound mutants, *in vivo*.

Materials and methods

Mouse strains and embryos

Sost$^{-/-}$ and *Sostdc1*$^{-/-}$ mice were generated by replacing the open reading frame with the *LacZ* reporter as previously described (Collette et al., 2010; Tanaka et al., 2010). *Sost*$^{-/-}$; *Sostdc1*$^{-/-}$ were generated by mating *Sost*$^{-/-}$ and *Sostdc1*$^{-/-}$ mice; E9.5 to E17.5 embryos were collected at various embryonic stages and geno-typed by PCR. E0.5 of gestation was considered to be noon on the day a copulatory plug was observed. Embryos earlier than E12.0 were stage-confirmed by somite counting for all subsequent analyses. All animal experiments were carried out in PHS-assured facilities in accordance with guidelines set by the Animal Care and Use Committee at University of California-Berkeley and Lawrence Livermore National Laboratory.

Identification of orthology and paralogy relationships

Human, rat, mouse, cow, chicken, and zebrafish orthologs of SOSTDC1 and SOST were identified from the Homologene database (Sayers et al., 2012) Release 66. HomoloGene homology searches rely on both proteins and their corresponding DNA sequences alignments, as well as synteny information, when applicable, and have been shown to perform well in phylogenetic and functional analyses where high specificity is required (Altenhoff and Dessimoz, 2009). In the case of frog, which is not included in the Homologene database, we used tBLASTn and BLASTp with the human protein sequences of SOSTDC1 and SOST to search the nucleotide and protein databases in NCBI, respectively; we only considered sequences represented in the current RefSeq (Pruitt et al., 2012).

Whole-mount in situ hybridization

Whole-mount *in situ* hybridizations were carried out using standard procedures (Collette et al., 2010). Briefly, digoxigenin-labeled antisense RNA probes were generated to the desired RNA sequence and hybridized to whole-mount embryos. Expression was visualized by binding BM Purple (Roche) to an alkaline-phosphatase conjugated anti-Digoxigenin antibody (Roche). Antisense RNA probes for *Grem1* (*MluI-Sac*II fragment of NM_011824),

*Fgf*8 (PstI 3′cDNA and UTR fragment of NM_010205); (Crossley and Martin, 1995), *Shh (MscI-NarI* fragment of NM_009170); (Echelard et al., 1993) were generated as described (Hogan et al., 1994) with the following modification: proteinase K digestion was omitted for ectodermal or AER probes. Gli1 (NM_010296.2) probes were generated from gel-purified PCR fragments (*Gli1* 5′-TCCTCCTCTCATTCCACAGG-3′; 5′-TCCAGCTGAGTGT TGTCCAG-3′). A minimum of 4 embryos were used per genotype, per experiment.

LacZ stains

Embryos were dissected into ice-cold 1 × phosphate-buffered saline (PBS), pH 7.3 and fixed in 2% paraformaldehyde, 0.2% glutaraldehyde in 1 × PBS, 2 mM $MgCl_2$ at 4°C for 30 min to 1 h, followed by extensive rinsing in 1 × PBS, 2 mM $MgCl_2$. Embryos were stained overnight at 4°C in X-gal stain: 1 mg/ml X-gal, $MgCl_2$, 5 mM EGTA, 0.02% Nonidet P-40, 5 mM potassium ferro-cyanide, 5 mM potassium ferricyanide, in 1 × PBS, pH 7.3. Neonates and adults (6 months of age) were skinned, eviscerated, and fixed as whole animals in 4% Paraformaldehyde in 1× PBS, 2 mM $MgCl_2$ for 1 h at 4 °C followed by extensive rinsing and staining overnight (neonates) or 48 h (adults) at 4°C in LacZ staining solution, as for embryos. Prior to staining, adult bones were decalcified in 0.5 M EDTA, pH 7.3, by the weight loss-weight-gain method of decalcification endpoint determination. After staining, embryos were post-fixed in 4% paraformaldehyde in 1 × PBS, pH 7.3 at 4°C, and then cleared in glycerol for photography. For sectioning, neonate and adult tissues were post-fixed for 72 h in 4% paraformaldehyde, dehydrated and embedded into paraffin wax. Section were cut at 6 mm, baked at 42°C overnight, counterstained with Nuclear Fast Red and mounted with Permount for imaging.

Skeletal preparations

Skeletal preparations were carried out on neonate and adult mice (6 months of age) using Alcian Blue 8GX for cartilage and Alizarin Red S for bone as previously described (Collette et al., 2010); E12.5–E14.5 mouse embryos were stained with Alcian Blue 8GX for cartilage only (0.05% in 4% glacial acetic acid).

Lysotracker apoptosis stain

Embryos were dissected at E12.5 and E13.5 in Hank's balanced saline solution (HBSS) and placed in lysotracker staining solution (2.5 ml/ml in HBSS) for 30 min at 37°C. Embryos were washed with 1 × PBS (pH 7.3) 2 × and fixed overnight in 4% paraformaldehyde at 4°C and dehydrated in methanol and cleared in benzyl alcohol:benzyl benzonate (1:1) for photography.

Immunofluorescent antibody stain

Embryos were dissected at E12.5 into ice-cold PBS and fixed for 24 h in 4% paraformaldehyde at 4°C. Embryos were washed, dehydrated, and embedded into paraffin for sectioning. Slides were dewaxed and epitopes requiring antigen retrieval were incubated in Uni-Trieve (Innovex) for 30 min at 65°C unless otherwise indicated. Slides were blocked with 5% BSA/0.01% Triton X-100 (Sigma) or Rodent Block (Innovex, for mouse/rat monoclonal antibodies only), incubated in a humid chamber with primary antibody

overnight at room temperature [1:200, anti-Gli3 (abcam), 1:200, anti-activated beta-catenin clone 8E7 (Millipore)], washed, and incubated for 2 h with Alexa-fluor-labeled secondary antibody (1:1000, Invitrogen/Molecular Probes), washed, and mounted using Prolong Gold/Prolog Gold with DAPI (Invitrogen/Molecular Probes) for imaging. Images were acquired using single-channel fluorescent filters on a Leica DM5000 compound microscope using a Qimaging color CCD camera and ImagePro software. Goat polyclonal anti-Sclerostin antibody (1:200, R&D Systems, cat# AF1589) and anti-goat Alexa-Fluor 488 secondary antibody (1:1000, Molecular Probes, cat# A21467) were used to determine Sost localization on bone paraffin sections as previously described (Collette et al., 2012).

Microarray analysis

Microarray data analysis was performed using R programming platform and Bioconductor (Gentleman et al., 2004). Bioconductor package 'affy' (Gautier et al., 2004) was used for data quality assessment. Data preprocessing and normalization were performed using Robust Multi-chip Average (RMA) protocol (Irizarry et al., 2003). Differentially expressed genes were identified using the empirical Bayes method implemented in Linear Models for Micro-Array (LIMMA) (Smyth, 2004) package. Probes were mapped to genes using Affymetrix Mouse Genome 430 2.0 Array annotation data from Bioconductor annotation package 'mouse4302.db'. Fold change values were calculated as the ratio between the averages of normalized intensities of the two groups, *Sost*$^{-/-}$ *Sostdc1*$^{-/-}$ and wildtype. Fold change values for differentially expressed genes are reported in a log2 scale. Genes with fold change of 2 (log2 FC=1) or greater and *P-value* less than 0.05 were considered differentially expressed. Pathway enrichment analysis was performed using the Database for Annotation, Visualization and Integrated Discovery (DAVID) (Dennis et al., 2003; Huang da et al., 2009) and Kyoto Encyclopedia of Genes and Genomes (KEGG) option (Kanehisa et al., 2010). Pathways with EASE score, a modified Fisher Exact *p*-value less than 0.1 were considered as enriched. Microarray data is publicly available at NCBI (GS E44325).

Results

Sost and Sostdc1 arose as duplication/divergence events

The human genomic region containing SOSTDC1 protein on chr 7 is syntenic with the region containing SOST on chr 17 (Fig. 1). Both *SOSTDC1* and *SOST* genes are extremely well conserved in the descendants of the ancestral Euteleostomi. Earlier chordates show some evidence of a *SOSTDC1* or *SOST* ortholog, suggesting that the duplication event took place at least 500 million years ago and that the genes belong to an ancient gene family. Other genes that are neighbors of *SOSTDC1* also have paralogs in the neighborhood of its paralog *SOST*, and this is true in all analyzed genomes. Thus, *ETV1* and *MEOX2* are paralogs of *ETV4* and *MEOX1*, respectively. This situation is consistent with a large-scale, possibly genomic duplication event, such as those that took place in the vertebrate ancestor (Dehal and Boore, 2005). The duplication was followed by divergence, resulting in the present-day human SOSTDC1 and SOST sharing only 40–42% of their amino acids, with similarity spanning over 84–92% of the protein lengths. It is likely that additional paralogous genes in these syntenic regions have diverged beyond our ability to detect homology. Individually, each of the corresponding syntenic regions, including other genes

and their relative order, is remarkably well conserved in Euteleostomi, suggesting fixation of the duplicated genes after a period of rapid divergence. Only in one examined lineage, the amphibians represented by *X. tropicalis*, we find *Sost* to be absent, suggesting that the duplicated region has been lost in this lineage. Finally, the noncoding regions in the vicinity of *SOSTDC1* and *SOST* are not uniformly conserved; while *SOSTDC1* is surrounded by a high density of evolutionary conserved noncoding sequences in mammals, only a few of these elements are shared among amniotes, suggesting neo- or sub-functionalization of the gene; in contrast some noncoding elements in the vicinity of *SOST* are conserved not only among amniotes, but, to a less extent, in tetrapods and fish (Loots and Ovcharenko, 2007).

Sost and Sostdc1 have non-overlapping expression patterns during limb development

LacZ was used to determine *Sost* and *Sostdc1* expression in *Sost-LacZ* knock-in mice (referred to as $Sost^{LacZ}$ for expression analysis, $Sost^{-/-}$ for phenotype analysis) and *Sostdc1-LacZ* knock-in (referred to as $Sostdc1^{LacZ}$ for expression analysis, $Sostdc1^{-/-}$ for phenotype analysis). $Sost^{LacZ}$ was observed as early as E9.5 in the distal limb bud (Fig. 2A-A″). This expression is restricted to the ectoderm and is excluded from the apical ectodermal ridge (AER) and mesenchyme at all time points examined (Fig. 2A-F and b-d). $Sostdc1^{LacZ}$ emerges ectodermally at E10.5 in a small field on the posterior side of the limb near the zone of polarizing activity (ZPA) marked by sonic hedgehog *(Shh)* (Fig. 2h, corresponding *Shh* expression indicated in Fig. 6A). By E11.5 its expression is strongly present primarily in the mesenchyme of the proximal limb (Fig. 2I and i). By E12.5 *Sostdc1* expression activated in the cartilage template outlining the ribs, vertebrae and digits (Fig. 2J and j). As limb development progresses, $Sost^{LacZ}$ remains confined to the ectoderm, and by E14.5 its expression becomes fainter and restricted to the digits. In contrast, $Sostdc1^{LacZ}$ expands its expression domain, surrounding the condensing cartilage anlagen, and intensifying in the proximal limb. By E14.5 *Sostdc1* is highly expressed in the limb in regions that include cartilage templates of the digits, mesenchyme and primary hair germs that are ectodermal derived, but is omitted from the most distal tips of the digits.

At E10.5–11.5 both *Sost* and *Sostdc1* are expressed in the head and mark parts of the nervous system of the developing embryos, but *Sost* expression has some unique features. As early as E9.5 *Sost* marks a very thin layer of cells that line the edge of the neural folds (Fig. 2B, C and Sup. Fig. 1A). As the neural folds close, *Sost* expression becomes restricted to the base of the cerebellum (Fig. 2D-E), consistent with our previously results in the adult cerebellum (Collette et al., 2012). Along the trunk, at E11.5 *Sost* emerges symmetrically at the base of the spinal cord, at the level of the forelimbs (Fig. 2C; Sup. Fig. 1B and D) in a cluster of cells that likely mark the lateral motor neurons migrating into the limb. A zoomed in view allows the visualization of projections into the limb bud that resemble previously described projections of motor axons (Dasen et al., 2008) (Sup. Fig. 1D); by E13.5 *Sost* marks a network of axons that innervate the dorsal limb flank mesenchyme (Fig. 2E′; Sup. Fig. 1E), and appears near the base of the hindlimbs by E13.5 (Sup. Fig. 1C). *Sostdc1* outlines the branchial arches as early as E10.5 (Fig. 2H); it marks the otic vesicle (Fig. 2H) and by E14.5 it is highly expressed in the ear, the developing skin and hair follicles (Fig. 2L). The E14.5 *Sostdc1* ectodermal expression (Fig. 2L) is similar to the previously reported beta-catenin *LacZ* reporter strains (Zhang et al., 2012; Narhi et al., 2008).

Sost and Sostdc1 are expressed in adjacent tissues in the neonatal skeleton

Starting at E16.5, *Sost* expression becomes restricted primarily to the skeleton, while *Sostdc1* expression spreads over the ectoderm, marks the hair follicles (Laurikkala et al., 2003; Narhi et al., 2008), tooth germs (Laurikkala et al., 2003) and many soft tissues throughout the late embryo. In neonates *Sost* marks the axial and appendicular skeleton (Fig. 3A–B), while *Sostdc1* is more broadly expressed in the limb and other soft tissues adjacent to bone (Fig. 3A′–B′). In the neonatal bone, we find *Sost* expression primarily in a location consistent with osteocytes (Fig. 3C and c); no *Sostdc1* expression is detected in this cell type; however *Sostdc1* is highly expressed in the adjacent periosteum (Fig. 3C′ and c′), connective tissue, muscle, and periarticular chondrocytes of the epiphysis (Fig. 3D′), while Sost expression is missing in these tissue types (Fig. 3D). In the skull and jaw *Sost* marks putative osteoblasts and osteocytes cells in wholemount calvaria (Fig. 3E and e) while Sostdc1 is found in the membrane covering the calvaria (Fig. 3E′ and e′) and in the connective tissue surrounding the mandible (Fig. 3F′). Significant *Sostdc1* expression was also found in the peripheral nervous system and in intervertebral disks (Fig. 3B′). Other sites of Sost neonatal expression included specific regions of the cardiovascular system (Sup. Fig. 2B, b, C and c). *Sostdc1* was also found in the kidney and in the urogenital system in neonates.

Sostdc1 and Sost have broad tissue distribution in the adult

In adult tissues, *Sost* and *Sostdc1* expression domains comprehensively encompass nearly every organ system and tissue in the body. *Sost* is robustly expressed in the skeleton, primarily in osteocytes, but low levels of *Sost* expression were also detected in osteoblasts and osteoclasts (Sup. Fig. 3A and C). This expression is consistent with its previously described roles in bone formation (Collette et al., 2012; Li et al., 2008), B-cell maintenance in the bone marrow niche (Cain et al., 2012), as well as recent reports that *Sost* is expressed in osteoclasts of aged mice (Ota et al., 2013). Other sites of *Sost* expression included the epididymis and vas deferens of the testis (Sup. Fig. 4A and a), the pyloric sphincter (Sup. Fig. 4B), parts of the cerebellum (Sup. Fig. 4C and c) and the kidney (Sup. Fig. 4E and e). Contrary to previous reports, *Sost* expression was not detected in the liver or cartilage, suggesting some differences between human and mouse endogenous *Sost* expression (Geetha-Loganathan et al., 2010). However, *Sost* cartilage expression has recently been linked to osteoarthritis, and there is a possibility that *Sost* expression turns on in the articular cartilage in response to joint trauma (Chan et al., 2011).

Sost expression was also detected in a highly restricted cluster of cells in the heart (Sup. Fig. 2D, d, and e), and in the ascending aorta branches (carotid arteries) of both the neonatal and adult heart (Sup. Fig. 2B, C, b, c, and E). The cardiovascular neonatal expression we observed is consistent with previous reports where Sost expression was detected in the smooth muscle cells of the ascending aorta, aortic arch, brachiocephalic artery, common carotids, and pulmonary trunk (van Bezooijen et al., 2007a). In contrast, *Sostdc1* expression was present in the cardiac plexus that innervates the heart (Sup. Fig. 2F and f).

Sostdc1 expression, however, has not been fully characterized. *Sostdc1* is expressed in the skin and hair follicles (Fig. 4A and a–a′), in the brain (Fig. 4B and B′), the stomach and

intestines (Fig. 4C, C′, D and D′), pancreas (Fig. 4E and E′), kidney (Fig. 4F and F′), nerves (Fig. 4G and I), lungs (Fig. 4H), smooth and skeletal muscles (Fig. 4J and K), vasculature (Fig. 4L), the urogenital system, teeth, connective tissue and periosteum. Previously published reports have described several phenotypes associated with these expression domains including roles in tooth development (Kassai et al., 2005), hair follicle development (Narhi et al., 2008, 2012), urogenital system development (Maeda et al., 2007), kidney development and toxicity (Tanaka et al., 2008), and more recently pancreas metabolism (Henley et al., 2012). While *Sostdc1* expression has not been described in the context of muscle tissue, the robust intermittent expression pattern is consistent with a described role for WNT signaling in the identity of muscle fiber types (Tee et al., 2009; von Maltzahn et al., 2012).

Preaxial polydactyly in Sost$^{-/-}$; Sostdc1$^{-/-}$ mice

Sostdc1 has not been previously associated with functions during skeletal development and *Sostdc1*$^{-/-}$ mice do not exhibit any obvious limb patterning defects. In contrast, *Sost* has been described in limb development in the context of Sclerosteosis. Sclerosteosis patients show variably penetrant limb developmental anomalies in the autopod, with a range of phenotypes that include soft and/or bony tissue syndactyly of anterior digits, nail dysplasia and radial deviation of digits (Hamersma et al., 2003; Itin et al., 2001). We also recently described *SOST* gain-of-function mice where overexpression of *SOST* caused severe limb patterning defects (Collette et al., 2010). Upon closer examination of *Sost*$^{-/-}$ mice we found 4% of neonates to display all hand defects previously described for Sclerosteosis patients (Fig. 5B-B2; Table 1). In addition, both *Sost*$^{-/-}$ and *Sostdc1*$^{-/-}$ mice had varying degrees of ventral pigmentation and ectopic hair growth on the autopod (Fig. 5b′; Table 1). When *Sost*$^{-/-}$ mice were mated to *Sostdc1*$^{-/-}$ to generate double knockout mice, ∼50% of the double knockout embryos displayed hand defects. Also, a new autopod defect emerged consisting of preaxial polydactyly primarily of digit 1 and occasionally of digit 2 (Fig. 5C–C″ and C4–C4′). The accompanying syndactyly of anterior digits seen in Sclerosteosis occurred in 6% of the embryos, but was not statistically different from the single mutant (Table 1). The preaxial polydactyly was visualized as early as E11.5 of development, in the form of ectopic tissue thickening in the anterior limb, during digit specification and templating of the autopod and is evident as polydactyly by as early as E12.5 (Fig. 5C1, arrow). We observed varying degrees of duplication, from incomplete soft-tissue duplication, to duplication of multiple projections with or without bone, at the site of the expected first digit, and protruding from the ventral autopod, the majority of defective *Sost*$^{-/-}$; *Sostdc1*$^{-/-}$ adults had a rudimentary duplicated thumb (Fig. 5C4′ and C4″) or an occasional branching off digit 2 (Fig. 5C4).

Sox9 is expressed in committed chondroprogenitor cells and differentiated chondrocytes and has been previously shown to function as an essential regulator of chondrogenesis. When *Sox9* was expressed ectopically in *Sox9*-transgenic mice, the cell density of the anterior limb bud mesenchyme at the site of *Sox9* transgene expression increased around E13.5, and a nubbin emerged ∼E14.5 highly similar to the ectodermal protrusion observed in *Sost*$^{-/-}$; *Sostdc1*$^{-/-}$ autopods (Fig. 5C3) (Akiyama et al., 2007). The *Sox9* transgenics showed increased proliferation at *Sox9* ectopic sites and the subsequent differentiation of *Sox9*

positive cells into chondrocytes (Akiyama et al., 2007). To determine if *Sox9* is involved in the *Sost*$^{-/-}$; *Sostdc1*$^{-/-}$ autopod defect, we examined *Sox9* expression in E13.5 embryos. Expression of *Sox9* appeared reduced in *Sost*$^{-/-}$ and enhanced in *Sostdc1*$^{-/-}$ embryos, although these patterns are not associated with cartilage templating defects in the single mutants. In *Sost*$^{-/-}$; *Sostdc1*$^{-/-}$ autopods, ectopic expression of *Sox9* was observed in the anterior region of digit 1 (Fig. 5G) which corresponded to the site of digit 1 duplication.

Changes in Gli1/Gli3 expression promote ectopic Sox9 and polydactyly in Sost$^{-/-}$; Sostdc1$^{-/-}$

Digit 1 formation has been described as *Shh*-independent since *Shh*$^{-/-}$ mice are missing all but digit 1, however altered morphogen diffusion or ectopic *Shh* affects anterior digits and has been shown to cause digit duplication. A number of mouse mutants with preaxial polydactyly exhibit ectopic *Shh* expression in the anterior mesenchyme of the limb bud during development; these include *Extra toes* (Xt), *Strong's luxoid* (lst), *luxate*, *X-linked polydactyly*, *Rim4*, *Hemimelic extra toes*, as well as *Msx1*$^{-/-}$;*Msx2*$^{-/-}$ mutants (Bensoussan-Trigano et al., 2011; Buscher and Ruther, 1998; Chan et al., 1995; Masuya et al., 1995; Sharpe et al., 1999). In particular paired-type homeodomain transcription factor *Alx4* is expressed in the mesenchyme of the anterior limb, and when mutated causes preaxial polydactyly slightly more severe than the polydactyly observed in *Sost*$^{-/-}$; *Sostdc1*$^{-/-}$ mice. Since *Sostdc1* expression domain slightly overlaps the ZPA at E10.5 (Fig. 2H′) and *Alx4 as well as Msx1*$^{-/-}$;*Msx2*$^{-/-}$ mice display ectopic *Shh* in the anterior digit 1 field of the autopod, we first compared *Shh* expression in single and double mutant embryos to *WT* embryos.

Consistent with loss of *Shh* expression in *SOST*^{tg} limbs (Collette et al., 2010), the *Shh* field was expanded both anteriorly and distally in *Sost*$^{-/-}$ and *Sost*$^{-/-}$; *Sostdc1*$^{-/-}$ embryos as early as E10.5 of development; in double mutants, this was before the preaxial polydactyly was visually detected (Fig. 6A). *Shh* expression in E11.5 *Sost*$^{-/-}$; *Sostdc1*$^{-/-}$ limbs was estimated to be 3.66-fold above *WT* levels as determined by microarray expression analysis (Table 2). However, unlike other mutants with digit 1 polydactyly, we detected no ectopic *Shh* expression in the anterior region of the E10.5 or E11.5 autopod (Fig. 6A and D) in all *Sostdc1*$^{-/-}$; *Sostdc1*$^{-/-}$ embryos examined (N=28). Consistent with *Shh* expansion, *Grem1* domain was reduced posteriorly since *Shh* positive cells repress *Grem1* expression (Fig. 6B), and was also missing in the anterior mesenchyme where ectopic digits form in double mutants (Fig. 7K′ and K″), but this reduction did not translate into a significant quantitative change in *Grem1* expression by microarray analysis in the E11.5 limb (Log FC: 0.81, FC: 1.75, p-value: 0.37133).

SHH signaling utilizes *Gli* transcription factors to mediate anterior-posterior limb patterning, and these proteins can function as either activators or repressors of transcription. *Gli3*, which functions primarily as a repressor, but the full-length protein can also serve as an activator, has been suggested to be the main effector of SHH signaling. In the absence of *Gli3 repression*, anterior digits are duplicated and take on anterior digit character that is dependent on the timing of *Gli3* inactivation, such that inactivation at E10.5 causes digit 1 duplication highly similar to the phenotype observed in *Sost*$^{-/-}$; *Sostdc1*$^{-/-}$ (Bowers et al.,

2012). *Gli1*, a downstream transcriptional activator of SHH, while not deemed essential for limb development in single KOs, does contribute to the formation of a posterior tissue nubbin in *Gli1*$^{-/-}$; *Gli2*$^{-/-}$ autopods (Park et al., 2000), and has been shown to activate *Sox9* expression via a *Gli1*-dependent transcriptional regulatory element (Bien-Willner et al., 2007). Consistent with these previous observations, we find *Gli1* to be up-regulated in *Sost*$^{-/-}$; *Sostdc1*$^{-/-}$ at E11.5, through both a dramatic anterior expansion (Fig. 6E) as well as a 2.3-fold change in transcript levels. Quantitatively *Gli3* was reduced by 3.68-fold in *Sost*$^{-/-}$; *Sostdc1*$^{-/-}$ in E11.5 limbs (Table 2). Immunofluorescent stains for activated Gli3 confirmed a dramatic reduction of Gli3 activator in the ectoderm, mesenchyme and in the cartilage anlangen in the E12.5 *Sost*$^{-/-}$; *Sostdc1*$^{-/-}$ limbs (Fig. 7D–F). In addition we observed ectopic anterior *Hoxd13* expression (Fig. 7L′–L″) in E11.5 *Sost*$^{-/-}$; *Sostdc1*$^{-/-}$ limbs consistent with results described for a hypermorphic activator allele of *Gli3* that resulted in preaxial polydactyly (Wang et al., 2007). Comprehensively, these findings suggest that the preaxial polydactyly in *Sost*$^{-/-}$; *Sostdc1*$^{-/-}$ limbs is the result of altered SHH signaling that induces ectopic *Sox9* expression *via* Gli3 derepression to promote tissue nubbins or extra rudimentary copies of anterior digits.

Altered FGF and BMP signaling cause syndactyly in Sost$^{-/-}$; Sostdc1$^{-/-}$

Sostdc1 has been previously characterized as both a WNT- and BMP-antagonist (Henley et al., 2012; Murashima-Suginami et al., 2008; Tanaka et al., 2008), and ectodermal derived BMPs and Fgf8 have been shown to control interdigital apoptosis (Hernandez-Martinez et al., 2009), a mechanism involved in the establishment of both polydactyly and syndactyly. Consistent with previous findings that *Fgf8* expression promotes cell survival and growth in the distal limb mesenchyme and that *Fgf8* repression triggers interdigital apoptosis associated with syndactyly we found *Sost*$^{-/-}$; *Sostdc1*$^{-/-}$ embryos to display both an increase in *Fgf*8 expression characterized by disorganized expansion of the AER domain, as well as a disruption of the AER continuity characterized by speckled down-regulation of *Fgf8* primarily in the anterior region of the limb (Fig. 6C, F, and G). Quantitatively *Fgf*8 was found to be 2.43-fold above *WT* levels in *Sost*$^{-/-}$; *Sostdc1*$^{-/-}$ E11.5 forelimbs, while *Fgf* receptors 1 through 3 were down-regulated (Table 2). Since ~6% of *Sost*$^{-/-}$; *Sostdc1*$^{-/-}$ embryos display syndactyly of anterior digits, we examined whether regions of *Fgf8* down-regulation corresponded to a decrease in interdigital apoptosis, and found a reduction in apoptosis in the 1-2 interdigital field at E12.5 (Fig. 6I).

Since *Bmp2/4* restrict *Shh* expression and antagonize *Fgf* signaling in the early limb, and *Bmp7* induces cell death in the distal mesenchyme and inhibits *Fgf8* expression in the ectoderm at later developmental times, we examined whether members of the *Bmp* family are transcriptionally affected in *Sost*$^{-/-}$; *Sostdc1*$^{-/-}$ embryos. *In situ* hybridization for *Bmp4* and *Bmp7* showed a complete absence of expression in the AER of *Sost*$^{-/-}$; *Sostdc1*$^{-/-}$ embryos (Fig. 7M–N). Additionally, most *Bmp*-related transcripts were down-regulated in *Sost*$^{-/-}$; *Sostdc1*$^{-/-}$ E11.5 forelimbs suggesting an overall reduction in BMP-signaling in the limb (Table 2) which may account for both *Shh* up-regulation and *Fgf*8 ectodermal/mesenchymal expansion.

WNT signaling is both up- and down-regulated in Sost$^{-/-}$; Sostdc1$^{-/-}$ limbs

Sost and *Sostdc1* have been previously described as antagonists of both WNT and BMP signaling (Collette et al., 2010; Holdsworth et al., 2012; Krause et al., 2010; Tanaka et al., 2010; Winkler et al., 2003). Our previous work of examining limb defects in transgenic mice overexpressing *SOST* showed that the BatGal transgene, a reporter of canonical WNT signaling was down-regulated in the limb mesenchyme, in response to elevated levels of *SOST* in the limb ectoderm (Collette et al., 2010). This data suggested that *SOST* functions as a WNT antagonist in the limb, in gain-of-function transgenic mice. Based on these previous findings, we anticipated *Sost*$^{-/-}$; *Sostdc1*$^{-/-}$ limb buds to display elevated WNT and/or possibly BMP signaling.

To determine what signaling pathways are altered due to lack of *Sost* and *Sostdc1* in the limb, we compared gene expression between *Sost*$^{-/-}$; *Sostdc1*$^{-/-}$ and wildtype E11.5 forelimbs using Affymetrix gene expression arrays (Mouse Genome 430 2.0 Array). We found 1218 and 1701 transcripts to be more than 2-fold up- or down-regulated in *Sost*$^{-/-}$; *Sostdc1*$^{-/-}$ forelimbs ($p \leq 0.05$), respectively. Consistent with the molecular marker analysis and WNT signaling function, pathway analysis identified WNT and SHH signaling among the top most significantly enriched in up-regulated genes; while all significantly altered transcripts associated with the BMP and TGFb signaling pathways were down-regulated in *Sost*$^{-/-}$; *Sostdc1*$^{-/-}$ limbs (Table 2). Interestingly, the WNT signaling was also identified among the top enriched in down-regulated genes, with 16 transcripts dramatically reduced in *Sost*$^{-/-}$; *Sostdc1*$^{-/-}$ limbs (Table 2).

To further determine what changes in WNT signaling occurred as a relationship of the signal transduction from receptor to transcriptional targets, we mapped each transcriptionally altered transcript on the WNT signaling map in Fig. 8. We depicted known inhibitory relationships among molecules (either at the transcript or protein level) by red lines and positive relationships by blue lines. We also marked the genes with significant transcriptional changes identified in *Sost*$^{-/-}$; *Sostdc1*$^{-/-}$ E11.5 limb buds with a red star for down-regulated genes or a green star for up-regulated genes. Contrary to our hypothesis that both *Sost* and *Sostdc1* interfere with canonical WNT signaling, we found β-catenin (CTNNB1; Fig. 8; yellow box) transcript levels reduced by 5.27-fold. In addition we found two inhibitors of canonical WNT signaling: GSK3B and NLK to be significantly up-regulated, 4.22-and 3.51-fold, respectively; and hence to further contribute to blunting β-catenin activator function, in the *Sost*$^{-/-}$; *Sostdc1*$^{-/-}$ limbs. Immunofluorescent stains of E12.5 sectioned limbs showed a marked increase in both ectodermal and mesenchymal β-catenin activity in *Sost*$^{-/-}$ limbs, while *Sostdc1*$^{-/-}$ limbs had a slight reduction in mesenchyme. Consistent with the microarray expression data, the double knockouts exhibited a dramatic reduction in both ectodermal and mesenchymal activated β-catenin (Fig. 9). In addition, two known non-canonical WNT ligands, WNT5A and WNT6 were significantly up-regulated 2.86- and 2.23-folds, respectively, and so were several transcription factors known to activate downstream WNT targets, including TCF4, TCF12, Lef1, and BCL9, along with several known WNT target genes, CCND, ID2 and FN1 (Table 2). While the microarray data conclusively high-lighted WNT signaling as the only pathway significantly up-regulated, it also suggested that the phenotypes are driven by a β-catenin

independent mechanism, and likely facilitated by the overabundance of the two non-canonical WNT ligands.

Discussion

The WNT signaling pathway is involved in a broad range of developmental and physiological processes ranging from cell proliferation, cell fate, body axis determination, tissue morphogenesis, and tissue homeostasis. Thus, its dysregulation has been linked to multiple congenital and degenerative diseases, as well as cancer. *Sost* and *Sostdc1* have been previously described as WNT antagonists, and therefore loss and/or gain-of-function mutations in these molecules are likely to interfere with aspects of WNT signaling pathway involved in critical developmental and metabolic processes. Here we showed that both *Sost* and *Sostdc1* have a broad tissue distribution in both the developing embryo and the adult mouse, broadening our current understanding of their expression pattern and therefore highlighting new potential functional sites where these two molecules could interfere with WNT and/or other signaling pathways. Their adjacent expression domains in the developing limb show epithelial-mesenchymal interactions that overlap to influence anterior digit patterning, especially in that several genes do not appear to be differentially regulated by *in situ* hybridization in single mutants, but show altered expression only in $Sost^{-/-}$; $Sostdc1^{-/-}$ double mutants. Second, we establish that the combined lack of *Sost* and *Sostdc1* causes preaxial polydactyly through modulating SHH signaling, through *Gli3* transcriptional repression, up-regulation of *Gli1* and subsequent ectopic activation of *Sox9* in the digit 1 field. Ectopic *Sox9* expression in $Sost^{-/-}$; $Sostdc1^{-/-}$ mice is likely a consequence of misregulated limb patterning genes upstream of *Sox9*, since we show that patterning genes such as *Grem1*, *Fgf8* and *Shh* are misregulated in the developing limb of $Sost^{-/-}$; $Sostdc1^{-/-}$ mice but they remain unaffected in *Sox9* gain-of-function mutant (Akiyama et al., 2007). The phenotype we describe herein is highly similar to the recently described conditional inactivation of *Gli3* in the developing autopod using a Cre deletor under the control of *Hoxa13* locus (Lopez-Rios et al., 2012). In this study, Lopez-Rios et al. were able to show that *Gli3* acts in the anterior mesenchyme to restrict and terminate *Grem1* expression in the anterior autopod in a spatiotemporally controlled manner, to promote BMP-dependent exit of progenitors from the proliferation phase to the chondrogenic differentiation stage. This is consistent with our data that show increased Gli3 activation in the anterior limb restricts *Grem1* expression despite the lack of ectopic *Shh*. In the absence of *Gli3* repressor, chondrogenic differentiation is delayed, resulting in an accumulation and subsequent increase in the pool of chondrogenic progenitor cells, which ultimately create new digit fields in the anterior region of the autopod (Lopez-Rios et al., 2012).

Lopez-Rios et al. show that the timing of *Gli3* inactivation determines the severity of the polydactyly phenotype, which in turn is directly related to the duration of the proliferative expansion of the progenitor cells phase, such that conditional inactivation of *Gli3* using *Hoxa13-Cre* results in the dissipation of the Gli3 transcripts by E11.75, and subsequent duplication of digit 1 only (Lopez-Rios et al., 2012). This timing coincides with the emergence of *Sostdc1* in the limb, since *Sostdc1* expression initiates at E10.5 on the ventral side of the autopod and subsequently expands to the proximal region of the E11.5 autopod. The cumulative absence of *Sost* and *Sostdc1* from the developing limb represses *Gli3*

transcript levels by 3.68-fold which is sufficient to generate a phenotype highly similar to the removal of *Gli3* allele at ~E11.5. As loss of *Gli3* transcription results primarily in the loss of *Gli3* repressor, our data shows that increased *Gli3* activator without increased *Gli3* transcription induces a similar mild preaxial polydactyly phenotype, similar to a study that demonstrated a hypermorphic allele of *Gli3* increased the activator form of the protein and resulted in mild preaxial polydactyly (Wang et al., 2007).

The SHH/GREM1/AER-FGF feedback loop has been studied extensively and significant evidence exists that indicate that BMP activity is at low levels during the proliferative expansion of digit progenitors, but at higher levels during chondrogenic differentiation (Bandyopadhyay et al., 2006; Lopez-Rios et al., 2012), and that SHH modulates these downstream effects. In the present study, we show that WNT signaling events upstream of SHH can produce alterations in *Gli3* expression which ultimately result in the same chondrogenic differentiation defects that cause preaxial polydactyly, positioning components of WNT signaling as novel candidates for congenital malformations observed in patients with preaxial polydactyly. Finally, extensive gene network and pathway analysis revealed that the preaxial polydactyly phenotype observed in $Sost^{-/-}$; $Sostdc1^{-/-}$ limbs, while consistent with a lack of WNT inhibition molecular output, it is b-catenin independent, and likely to be mediated by two non-canonical WNT ligands: Wnt5A and Wnt6. In particular, since Wnt6 has been previously described as an ectodermally derived negative regulator of chondrogenesis (Geetha-Loganathan et al., 2010), the link between *Sost*, *Sostdc1*, and *Wnt6*, chondrogenic differentiation and proliferation should be further explored.

Supplementary Material

Refer to Web version on PubMed Central for supplementary material.

Acknowledgments

We would like to thank the National Institutes of Health (NIH) Knock-Out Mouse Program (KOMP) and Regeneron for providing the *Sost* and *Sostdc1* knockout mice. NMC, CY, DM and GGL were supported by NIH Grant HD47853 and DK075730. This work was performed under the auspices of the U.S. Department of Energy by Lawrence Livermore National Laboratory under Contract DE-AC52-07NA27344. LT was supported by the Intramural Research Program of the NIH, NLM.

References

Ahn Y, Sanderson BW, Klein OD, Krumlauf R. Inhibition of Wnt signaling by Wise (Sostdc1) and negative feedback from Shh controls tooth number and patterning. Development. 2010; 137:3221–3231. [PubMed: 20724449]

Akiyama H, Stadler HS, Martin JF, Ishii TM, Beachy PA, Nakamura T, de Crombrugghe B. Misexpression of Sox9 in mouse limb bud mesenchyme induces polydactyly and rescues hypodactyly mice. Matrix Biol: J Int Soc Matrix Biol. 2007; 26:224–233.

Altenhoff AM, Dessimoz C. Phylogenetic and functional assessment of orthologs inference projects and methods. PLoS Comput Biol. 2009; 5:e1000262. [PubMed: 19148271]

Balemans W, Ebeling M, Patel N, Van Hul E, Olson P, Dioszegi M, Lacza C, Wuyts W, Van Den Ende J, Willems P, Paes-Alves AF, Hill S, Bueno M, Ramos FJ, Tacconi P, Dikkers FG, Stratakis C, Lindpaintner K, Vickery B, Foernzler D, Van Hul W. Increased bone density in sclerosteosis is due to the deficiency of a novel secreted protein (SOST). Hum Mol Genet. 2001; 10:537–543. [PubMed: 11181578]

Bandyopadhyay A, Tsuji K, Cox K, Harfe BD, Rosen V, Tabin CJ. Genetic analysis of the roles of BMP2, BMP4, and BMP7 in limb patterning and skeletogenesis. PLoS Genet. 2006; 2:e216. [PubMed: 17194222]

Bensoussan-Trigano V, Lallemand Y, Saint Clement C, Robert B. Msx1 and Msx2 in limb mesenchyme modulate digit number and identity. Dev Dyn. 2011; 240:1190–1202. [PubMed: 21465616]

Bien-Willner GA, Stankiewicz P, Lupski JR. SOX9cre1, a cis-acting regulatory element located 1.1 Mb upstream of SOX9, mediates its enhancement through the SHH pathway. Hum Mol Genet. 2007; 16:1143–1156. [PubMed: 17409199]

Blish KR, Clausen KA, Hawkins GA, Garvin AJ, Willingham MC, Turner JC, Torti FM, Torti SV. Loss of heterozygosity and SOSTDC1 in adult and pediatric renal tumors. J Exp Clin Cancer Res: CR. 2010; 29:147. [PubMed: 21080955]

Bowers M, Eng L, Lao Z, Turnbull RK, Bao X, Riedel E, Mackem S, Joyner AL. Limb anterior–posterior polarity integrates activator and repressor functions of GLI2 as well as GLI3. Dev Biol. 2012; 370:110–124. [PubMed: 22841643]

Buscher D, Ruther U. Expression profile of Gli family members and Shh in normal and mutant mouse limb development. Dev Dyn. 1998; 211:88–96. [PubMed: 9438426]

Cain CJ, Rueda R, McLelland B, Collette NM, Loots GG, Manilay JO. Absence of sclerostin adversely affects B cell survival. J Bone Miner Res. 2012; 27:1451–1461. [PubMed: 22434688]

Chan BY, Fuller ES, Russell AK, Smith SM, Smith MM, Jackson MT, Cake MA, Read RA, Bateman JF, Sambrook PN, Little CB. Increased chondrocyte sclerostin may protect against cartilage degradation in osteoarthritis. Osteoarthritis Cartilage. 2011; 19:874–885. [PubMed: 21619935]

Chan DC, Laufer E, Tabin C, Leder P. Polydactylous limbs in Strong's Luxoid mice result from ectopic polarizing activity. Development. 1995; 121:1971–1978. [PubMed: 7635045]

Collette NM, Genetos DC, Economides AN, Xie L, Shahnazari M, Yao W, Lane NE, Harland RM, Loots GG. Targeted deletion of Sost distal enhancer increases bone formation and bone mass. Proc Natl Acad Sci USA. 2012; 109:14092–14097. [PubMed: 22886088]

Collette NM, Genetos DC, Murugesh D, Harland RM, Loots GG. Genetic evidence that SOST inhibits WNT signaling in the limb. Dev Biol. 2010; 342:169–179. [PubMed: 20359476]

Crossley PH, Martin GR. The mouse Fgf8 gene encodes a family of polypeptides and is expressed in regions that direct outgrowth and patterning in the developing embryo. Development. 1995; 121:439–451. [PubMed: 7768185]

Dasen JS, De Camilli A, Wang B, Tucker PW, Jessell TM. Hox repertoires for motor neuron diversity and connectivity gated by a single accessory factor, FoxP1. Cell. 2008; 134:304–316. [PubMed: 18662545]

Dehal P, Boore JL. Two rounds of whole genome duplication in the ancestral vertebrate. PLoS Biol. 2005; 3:e314. [PubMed: 16128622]

Dennis G Jr, Sherman BT, Hosack DA, Yang J, Gao W, Lane HC, Lempicki RA. DAVID: database for annotation, visualization, and integrated discovery. Genome Biol. 2003; 4:3.

Echelard Y, Epstein DJ, St-Jacques B, Shen L, Mohler J, McMahon JA, McMahon AP. Sonic hedgehog, a member of a family of putative signaling molecules, is implicated in the regulation of CNS polarity. Cell. 1993; 75:1417–1430. [PubMed: 7916661]

Gautier L, Cope L, Bolstad BM, Irizarry RA. Affy—analysis of Affymetrix GeneChip data at the probe level. Bioinformatics. 2004; 20:307–315. [PubMed: 14960456]

Geetha-Loganathan P, Nimmagadda S, Christ B, Huang R, Scaal M. Ectodermal Wnt6 is an early negative regulator of limb chondrogenesis in the chicken embryo. BMC Dev Biol. 2010; 10:32. [PubMed: 20334703]

Gentleman RC, Carey VJ, Bates DM, Bolstad B, Dettling M, Dudoit S, Ellis B, Gautier L, Ge Y, Gentry J, Hornik K, Hothorn T, Huber W, Iacus S, Irizarry R, Leisch F, Li C, Maechler M, Rossini AJ, Sawitzki G, Smith C, Smyth G, Tierney L, Yang JY, Zhang J. Bioconductor: open software development for computational biology and bioinformatics. Genome Biol. 2004; 5:R80. [PubMed: 15461798]

Hamersma H, Gardner J, Beighton P. The natural history of sclerosteosis. Clin Genet. 2003; 63:192–197. [PubMed: 12694228]

He JW, Yue H, Hu WW, Hu YQ, Zhang ZL. Contribution of the sclerostin domain-containing protein 1 (SOSTDC1) gene to normal variation of peak bone mineral density in Chinese women and men. J Bone Miner Metab. 2011; 29:571–581. [PubMed: 21221677]

Henley KD, Gooding KA, Economides AN, Gannon M. Inactivation of the dual Bmp/Wnt inhibitor Sostdc1 enhances pancreatic islet function. Am J Physiol Endocrinol Metab. 2012; 303:E752–E761. [PubMed: 22829579]

Hernandez-Martinez R, Castro-Obregon S, Covarrubias L. Progressive interdigital cell death: regulation by the antagonistic interaction between fibroblast growth factor 8 and retinoic acid. Development. 2009; 136:3669–3678. [PubMed: 19820185]

Hoffmann FG, Storz JF, Gorr TA, Opazo JC. Lineage-specific patterns of functional diversification in the alpha- and beta-globin gene families of tetrapod vertebrates. Mol Biol Evol. 2010; 27:1126–1138. [PubMed: 20047955]

Hogan, BL.; Beddington, R.; Costantini, F.; Lacey, E. Manipulating the Mouse Embryo: A Laboratory Manual. 2nd. Cold Spring Harbor Press; New York: 1994.

Holdsworth G, Slocombe P, Doyle C, Sweeney B, Veverka V, Le Riche K, Franklin RJ, Compson J, Brookings D, Turner J, Kennedy J, Garlish R, Shi J, Newnham L, McMillan D, Muzylak M, Carr MD, Henry AJ, Ceska T, Robinson MK. Characterization of the interaction of sclerostin with the low density lipoprotein receptor-related protein (LRP) family of Wnt co-receptors. J Biol Chem. 2012; 287:26464–26477. [PubMed: 22696217]

Huang da W, Sherman BT, Lempicki RA. Systematic and integrative analysis of large gene lists using DAVID bioinformatics resources. Nat Protocols. 2009; 4:44–57. [PubMed: 19131956]

Irizarry RA, Hobbs B, Collin F, Beazer-Barclay YD, Antonellis KJ, Scherf U, Speed TP. Exploration, normalization, and summaries of high density oligonucleotide array probe level data. Biostatistics. 2003; 4:249–264. [PubMed: 12925520]

Itin PH, Keseru B, Hauser V. Syndactyly/brachyphalangy and nail dysplasias as marker lesions for sclerosteosis. Dermatology. 2001; 202:259–260. [PubMed: 11385236]

Jarvinen E, Tummers M, Thesleff I. The role of the dental lamina in mammalian tooth replacement. J Exp Zool Part B, Mol Dev Evol. 2009; 312B:281–291.

Kanehisa M, Goto S, Furumichi M, Tanabe M, Hirakawa M. KEGG for representation and analysis of molecular networks involving diseases and drugs. Nucleic Acids Res. 2010; 38:D355–D360. [PubMed: 19880382]

Kassai Y, Munne P, Hotta Y, Penttila E, Kavanagh K, Ohbayashi N, Takada S, Thesleff I, Jernvall J, Itoh N. Regulation of mammalian tooth cusp patterning by ectodin. Science. 2005; 309:2067–2070. [PubMed: 16179481]

Krause C, Korchynskyi O, de Rooij K, Weidauer SE, de Gorter DJ, van Bezooijen RL, Hatsell S, Economides AN, Mueller TD, Lowik CW, ten Dijke P. Distinct modes of inhibition by sclerostin on bone morphogenetic protein and Wnt signaling pathways. J Biol Chem. 2010; 285:41614–41626. [PubMed: 20952383]

Kusu N, Laurikkala J, Imanishi M, Usui H, Konishi M, Miyake A, Thesleff I, Itoh N. Sclerostin is a novel secreted osteoclast-derived bone morpho-genetic protein antagonist with unique ligand specificity. J Biol Chem. 2003; 278:24113–24117. [PubMed: 12702725]

Laurikkala J, Kassai Y, Pakkasjarvi L, Thesleff I, Itoh N. Identification of a secreted BMP antagonist, ectodin, integrating BMP, FGF, and SHH signals from the tooth enamel knot. Dev Biol. 2003; 264:91–105. [PubMed: 14623234]

Li X, Ominsky MS, Niu QT, Sun N, Daugherty B, D'Agostin D, Kurahara C, Gao Y, Cao J, Gong J, Asuncion F, Barrero M, Warmington K, Dwyer D, Stolina M, Morony S, Sarosi I, Kostenuik PJ, Lacey DL, Simonet WS, Ke HZ, Paszty C. Targeted deletion of the sclerostin gene in mice results in increased bone formation and bone strength. J Bone Miner Res. 2008; 23:860–869. [PubMed: 18269310]

Li X, Zhang Y, Kang H, Liu W, Liu P, Zhang J, Harris SE, Wu D. Sclerostin binds to LRP5/6 and antagonizes canonical Wnt signaling. J Biol Chem. 2005; 280:19883–19887. [PubMed: 15778503]

Lintern KB, Guidato S, Rowe A, Saldanha JW, Itasaki N. Characterization of wise protein and its molecular mechanism to interact with both Wnt and BMP signals. J Biol Chem. 2009; 284:23159–23168. [PubMed: 19553665]

Loots G, Ovcharenko I. ECRbase: database of evolutionary conserved regions, promoters, and transcription factor binding sites in vertebrate genomes. Bioinformatics. 2007; 23:122–124. [PubMed: 17090579]

Lopez-Rios J, Speziale D, Robay D, Scotti M, Osterwalder M, Nusspaumer G, Galli A, Hollander GA, Kmita M, Zeller R. GLI3 constrains digit number by controlling both progenitor proliferation and BMP-dependent exit to chondrogenesis. Dev Cell. 2012; 22:837–848. [PubMed: 22465667]

Maeda K, Lee DS, Yanagimoto Ueta Y, Suzuki H. Expression of uterine sensitization-associated gene-1 (USAG-1) in the mouse uterus during the periimplantation period. J Reprod Dev. 2007; 53:931–936. [PubMed: 17389776]

Masuya H, Sagai T, Wakana S, Moriwaki K, Shiroishi T. A duplicated zone of polarizing activity in polydactylous mouse mutants. Genes Dev. 1995; 9:1645–1653. [PubMed: 7628698]

Moleirinho A, Carneiro J, Matthiesen R, Silva RM, Amorim A, Azevedo L. Gains, losses and changes of function after gene duplication: study of the metallothionein family. PLoS One. 2011; 6:e18487. [PubMed: 21541013]

Munne PM, Tummers M, Jarvinen E, Thesleff I, Jernvall J. Tinkering with the inductive mesenchyme: Sostdc1 uncovers the role of dental mesenchyme in limiting tooth induction. Development. 2009; 136:393–402. [PubMed: 19141669]

Murashima-Suginami A, Takahashi K, Sakata T, Tsukamoto H, Sugai M, Yanagita M, Shimizu A, Sakurai T, Slavkin HC, Bessho K. Enhanced BMP signaling results in supernumerary tooth formation in USAG-1 deficient mouse. Biochem Biophys Res Commun. 2008; 369:1012–1016. [PubMed: 18329379]

Narhi K, Jarvinen E, Birchmeier W, Taketo MM, Mikkola ML, Thesleff I. Sustained epithelial beta-catenin activity induces precocious hair development but disrupts hair follicle down-growth and hair shaft formation. Development. 2008; 135:1019–1028. [PubMed: 18256193]

Narhi K, Tummers M, Ahtiainen L, Itoh N, Thesleff I, Mikkola ML. Sostdc1 defines the size and number of skin appendage placodes. Dev Biol. 2012; 364:149–161. [PubMed: 22509524]

Ota K, Quint P, Ruan M, Pederson L, Westendorf JJ, Khosla S, Oursler MJ. Sclerostin is expressed in osteoclasts from aged mice and reduces osteoclast-mediated stimulation of mineralization. J Cell Biochem. 2013; 114:1901–1907. [PubMed: 23494985]

Park HL, Bai C, Platt KA, Matise MP, Beeghly A, Hui CC, Nakashima M, Joyner AL. Mouse Gli1 mutants are viable but have defects in SHH signaling in combination with a Gli2 mutation. Development. 2000; 127:1593–1605. [PubMed: 10725236]

Pruitt KD, Tatusova T, Brown GR, Maglott DR. NCBI Reference Sequences (RefSeq): current status, new features and genome annotation policy. Nucleic Acids Res. 2012; 40:D130–D135. [PubMed: 22121212]

Sayers EW, Barrett T, Benson DA, Bolton E, Bryant SH, Canese K, Chetvernin V, Church DM, Dicuccio M, Federhen S, Feolo M, Fingerman IM, Geer LY, Helmberg W, Kapustin Y, Krasnov S, Landsman D, Lipman DJ, Lu Z, Madden TL, Madej T, Maglott DR, Marchler-Bauer A, Miller V, Karsch-Mizrachi I, Ostell J, Panchenko A, Phan L, Pruitt KD, Schuler GD, Sequeira E, Sherry ST, Shumway M, Sirotkin K, Slotta D, Souvorov A, Starchenko G, Tatusova TA, Wagner L, Wang Y, Wilbur WJ, Yaschenko E, Ye J. Database resources of the National Center for Biotechnology Information. Nucleic Acids Res. 2012; 40:D13–D25. [PubMed: 22140104]

Semenov M, Tamai K, He X. SOST is a ligand for LRP5/LRP6 and a Wnt signaling inhibitor. J Biol Chem. 2005; 280:26770–26775. [PubMed: 15908424]

Sharpe J, Lettice L, Hecksher-Sorensen J, Fox M, Hill R, Krumlauf R. Identification of sonic hedgehog as a candidate gene responsible for the polydactylous mouse mutant Sasquatch. Curr Biol. 1999; 9:97–100. [PubMed: 10021368]

Smyth GK. Linear models and empirical bayes methods for assessing differential expression in microarray experiments. Stat Appl Genet Mol Biol. 2004; 3 Article 3.

Sugiura Y, Yasuhara T. Sclerosteosis a case report. J Bone J Surg Am. 1975; 57:273–277.

Tanaka M, Asada M, Higashi AY, Nakamura J, Oguchi A, Tomita M, Yamada S, Asada N, Takase M, Okuda T, Kawachi H, Economides AN, Robertson E, Takahashi S, Sakurai T, Goldschmeding R, Muso E, Fukatsu A, Kita T, Yanagita M. Loss of the BMP antagonist USAG-1 ameliorates disease

in a mouse model of the progressive hereditary kidney disease Alport syndrome. J Clin Invest. 2010; 120:768–777. [PubMed: 20197625]

Tanaka M, Endo S, Okuda T, Economides AN, Valenzuela DM, Murphy AJ, Robertson E, Sakurai T, Fukatsu A, Yancopoulos GD, Kita T, Yanagita M. Expression of BMP-7 and USAG-1 (a BMP antagonist) in kidney development and injury. Kidney Int. 2008; 73:181–191. [PubMed: 17943079]

Tee JM, van Rooijen C, Boonen R, Zivkovic D. Regulation of slow and fast muscle myofibrillogenesis by Wnt/beta-catenin and myostatin signaling. PLoS One. 2009; 4:e5880. [PubMed: 19517013]

ten Dijke P, Krause C, de Gorter DJ, Lowik CW, van Bezooijen RL. Osteocyte-derived sclerostin inhibits bone formation: its role in bone morphogenetic protein and Wnt signaling. J Bone J Surg Am. 2008; 90(Suppl 1):31–35.

Turk T, Leeuwis JW, Gray J, Torti SV, Lyons KM, Nguyen TQ, Goldschmeding R. BMP signaling and podocyte markers are decreased in human diabetic nephropathy in association with CTGF overexpression. J Histochem Cytochem: Off J Histochem Soc. 2009; 57:623–631.

van Bezooijen RL, Deruiter MC, Vilain N, Monteiro RM, Visser A, van der Wee-Pals L, van Munsteren CJ, Hogendoorn PC, Aguet M, Mummery CL, Papapoulos SE, Ten Dijke P, Lowik CW. SOST expression is restricted to the great arteries during embryonic and neonatal cardiovascular development. Dev Dyn. 2007a; 236:606–612. [PubMed: 17195180]

van Bezooijen RL, Svensson JP, Eefting D, Visser A, van der Horst G, Karperien M, Quax PH, Vrieling H, Papapoulos SE, ten Dijke P, Lowik CW. Wnt but not BMP signaling is involved in the inhibitory action of sclerostin on BMP-stimulated bone formation. J Bone Miner Res. 2007b; 22:19–28. [PubMed: 17032150]

van Bezooijen RL, ten Dijke P, Papapoulos SE, Lowik CW. SOST/sclerostin, an osteocyte-derived negative regulator of bone formation. Cytokine Growth Factor Rev. 2005; 16:319–327. [PubMed: 15869900]

von Maltzahn J, Renaud JM, Parise G, Rudnicki MA. Wnt7a treatment ameliorates muscular dystrophy. Proc Natl Acad Sci USA. 2012; 109:20614–20619. [PubMed: 23185011]

Wang C, Pan Y, Wang B. A hypermorphic mouse Gli3 allele results in a polydactylous limb phenotype. Dev Dyn. 2007; 236:769–776. [PubMed: 17266131]

Winkler DG, Sutherland MK, Geoghegan JC, Yu C, Hayes T, Skonier JE, Shpektor D, Jonas M, Kovacevich BR, Staehling-Hampton K, Appleby M, Brunkow ME, Latham JA. Osteocyte control of bone formation via sclerostin, a novel BMP antagonist. Embo J. 2003; 22:6267–6276. [PubMed: 14633986]

Yanagita M, Okuda T, Endo S, Tanaka M, Takahashi K, Sugiyama F, Kunita S, Takahashi S, Fukatsu A, Yanagisawa M, Kita T, Sakurai T. Uterine sensitization-associated gene-1 (USAG-1), a novel BMP antagonist expressed in the kidney, accelerates tubular injury. J Clin Invest. 2006; 116:70–79. [PubMed: 16341262]

Zhang M, Shi J, Huang Y, Lai L. Expression of canonical WNT/beta-CATENIN signaling components in the developing human lung. BMC Dev Biol. 2012; 12:21. [PubMed: 22846383]

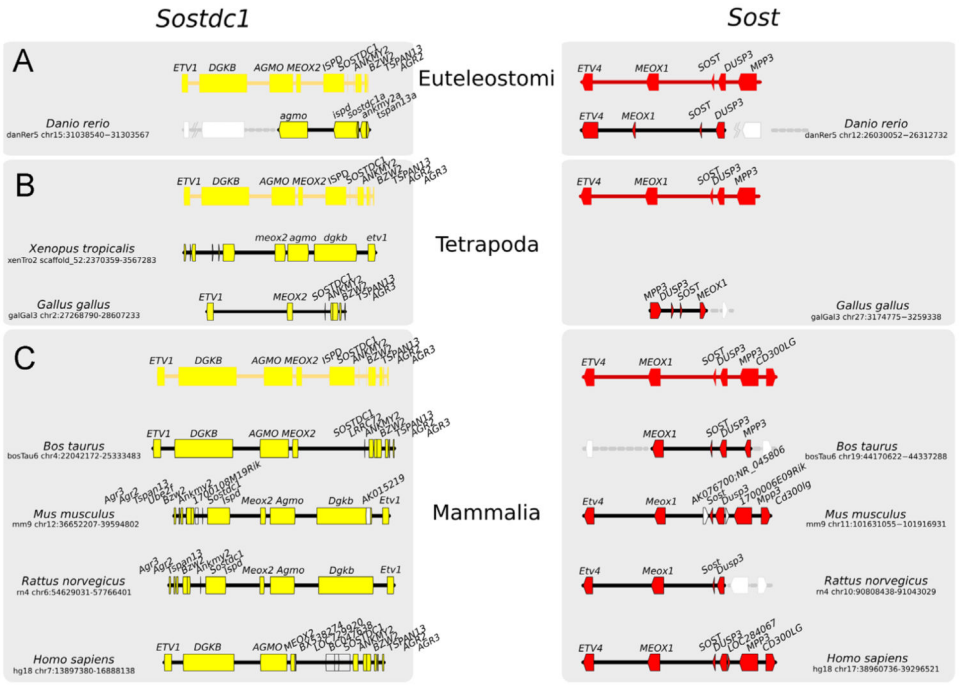

Fig. 1.

Sost–Sostdc1 evolutionary relationship. An overview of SOSTDC1 (left) and SOST (right) evolution, created by tracking the SOSTDC1 and SOST gene loci through representative vertebrate genomes (not to scale) from (A) Euteleostomi, (B) Tetrapoda and (C) Mammals clades. Predicted orthologs (where annotation is not available) are shown with gray dotted lines. Genes are shown as arrowheads, with their gene symbols above. Genes that are not conserved/likely to be poorly annotated are represented in white. The direction of the arrowhead indicates the relative transcriptional orientation and the relevant genome coordinates indicated on the left and right respectively.

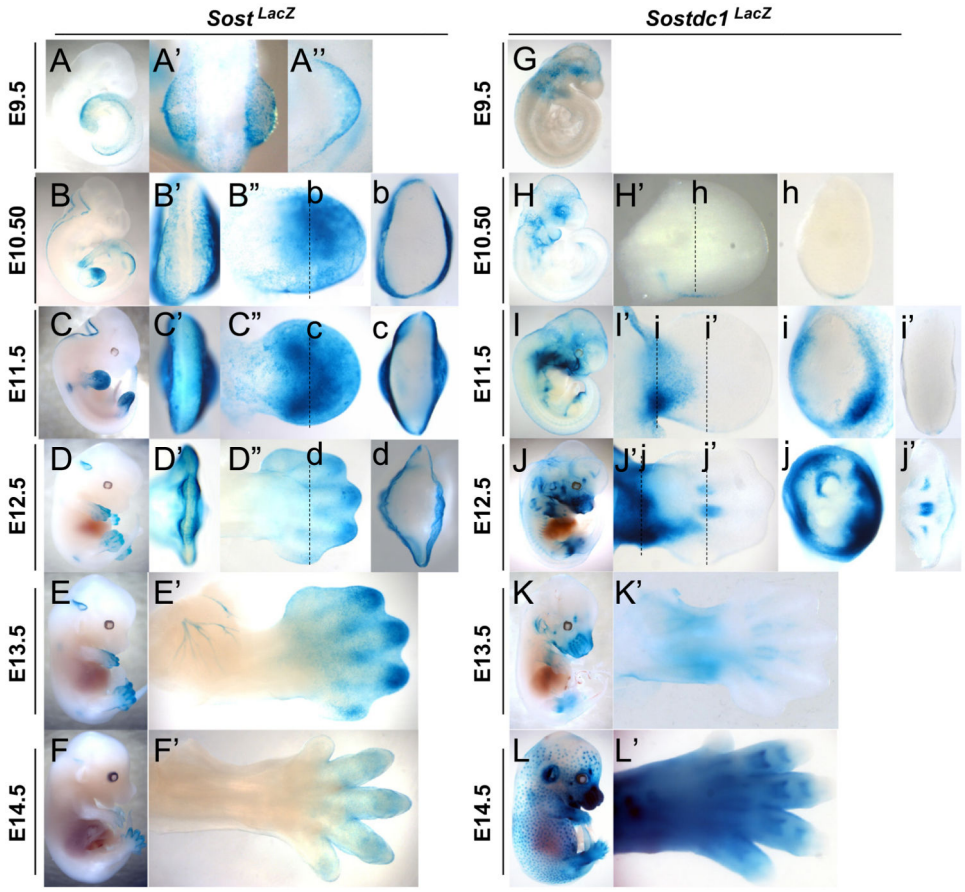

Fig. 2.

Sost and *Sostdc1* expression during limb development visualized by LacZ expression. *Sost* (A–F) and *Sostdc1* (G–L) expressions were examined in a time-course panel of E9.5–E14.5 heterozygous embryos referred to as $Sost^{LacZ}$ and $Sostdc1^{LacZ}$. At E9.5 in $Sost^{LacZ}$ embryos, a dorsal view of the whole embryo (A′) and of the forelimb (A″) shows expression in the emerging limb bud while no limb expression is detected in $Sostdc1^{LacZ}$ (G). For E10.5 to E12.5 embryos (B–D and H–J), AER views (B′–D′), dorsal limb views (B″–D″ and H′–J′) and transverse section views (b–d; h–j; and i′, j′) are provided. For E13.5 and E14.5 embryos (E–F; K–L), dorsal limb views (E′–F′; K′–L′) are provided.

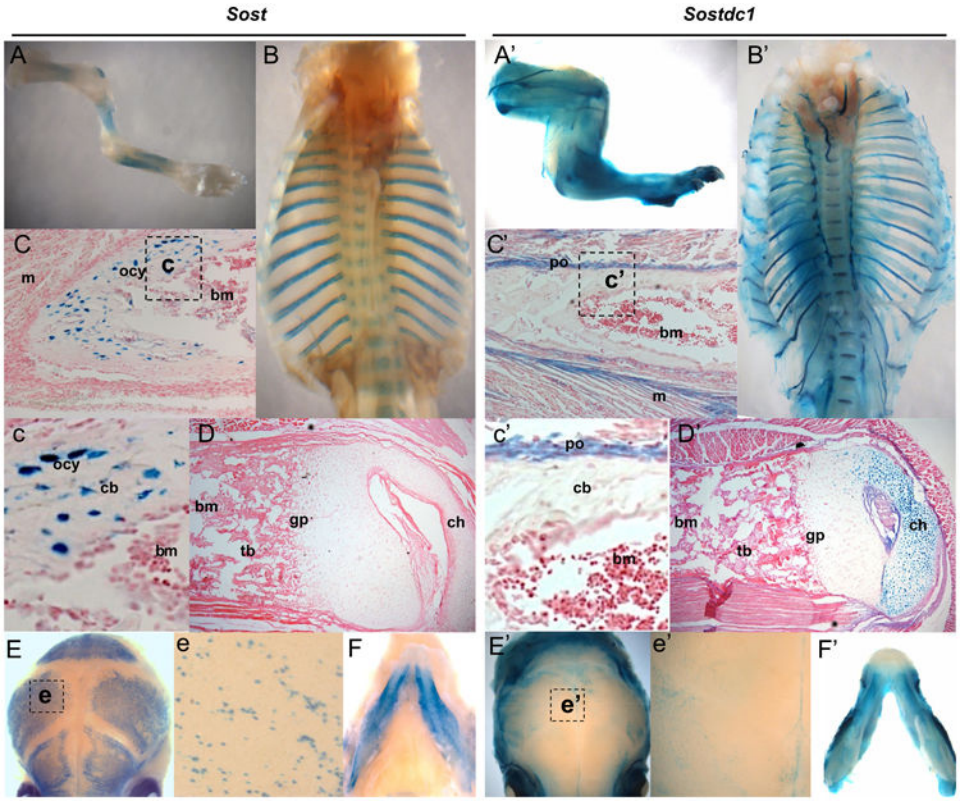

Fig. 3.

Sost and *Sostdc1* expression in the neonatal skeleton. *Sost* expression marked cells in the appendicular (A) and axial (B, E) skeleton, while *Sostdc1* was more broadly expressed in the limbs (A′) and rib cage (B′) to encompass connective tissue, muscle, cartilage and neurons. Sectioned long bones revealed *Sost* expression primarily in the osteocytes of cortical bone (C and c), but no obvious *Sost* expression was detected in the articular cartilage (D). *Sostdc1* however was not detected in the mineralized bone; it was expressed in the periosteum (C and c′), the immediately adjacent muscles (C′) and the periarticular chondrocytes in the condyle (D′). Both *Sost* and *Sostdc1* were also detected in the skull (E and E′) and mandible (F and F ′); *Sost* expression was localized to osteoblasts and osteocytes in wholemount calvaria (e), while *Sostdc1* was present in the connective tissue over the calvarial bones (e′); and *m* muscle; *ocy* osteocytes; *bm* bone marrow; *po* periosteum; *cb* cortical bone; *gp* growth plate; and *ch* chondrocytes.

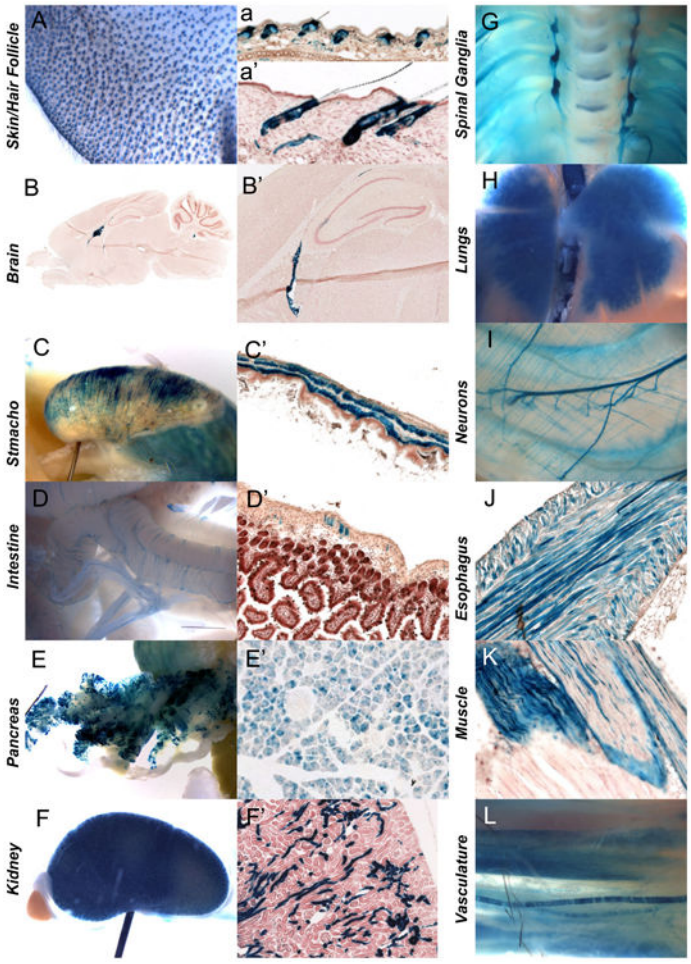

Fig. 4.

Sostdc1 expression in adult tissues. Sostdc1 expression was examined in wholemount and sectioned LacZ stained tissues, and was detected in the skin and hair follicles (A, a, and a′). A highly specialized region in the brain was positive for *Sostdc1* (B and B′). Smooth muscles of the stomach (C and C′), intestine (D and D′) and esophagus (J), and skeletal muscle (K) expressed *Sostdc1*. Sostdc1 was also robustly expressed in the pancreas (E and E′) and kidney (F and F′) and in the nervous system Sostdc1 stained spinal ganglia (G) and the lungs (H). Neurons (I) and vasculature was also positive for Sostdc1 (L).

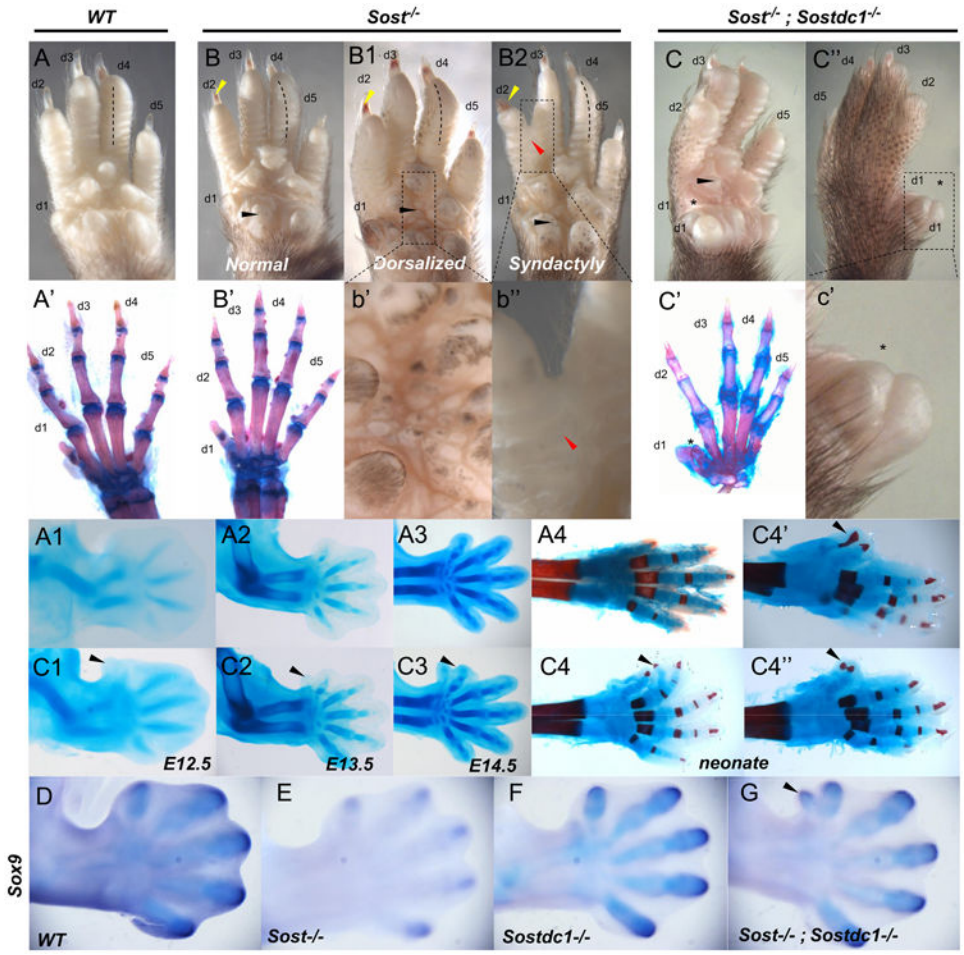

Fig. 5.

Limb defects in *Sost*$^{-/-}$ and *Sost*$^{-/-}$; *Sostdc1*$^{-/-}$ mice. Compared to adult *WT* autopods (A), *Sost*$^{-/-}$ autopods (B, B1, and B2, insets at b′ and b″) displayed pigmentation on the ventral side (B1 and b′), digit 2–3 syndactyly (B2 and b″; red arrow), nail dysplasia (B, B1 and B2; yellow arrows) and radial deviation of digits, primarily observed for digit 4 (B, B1 and B2, dotted lines). Ventral pigmentation was also observed in *Sost*$^{-/-}$; *Sostdc1*$^{-/-}$ autopods. Unlike *WT* and *Sost*$^{-/-}$ autopods that had normal digit patterning (A′–B′), *Sost*$^{-/-}$; *Sostdc1*$^{-/-}$ digit 1 was thicker (C, C″ and c′; asterisk) and skeletal preparation indicated the presence of extra bones (C′) in digit 1. A time course skeletal preparation examination revealed that an ectopic digit 1 was distinguishable as a tissue projection as early as E12.5 (A1-3 *vs.* C1-3); and the neonate *Sost*$^{-/-}$; *Sostdc1*$^{-/-}$ limbs displayed a range of extra digits (C4 and C4″) associated with ectopic projections primarily from digit 1 (C4′ and C4″) and in rare occasions from digit 2 (C4; black arrow). Sox9 *in situ* hybridization on E13 embryos revealed an ectopic digit 1 field in *Sost*$^{-/-}$; *Sostdc1*$^{-/-}$ autopods. d digit.

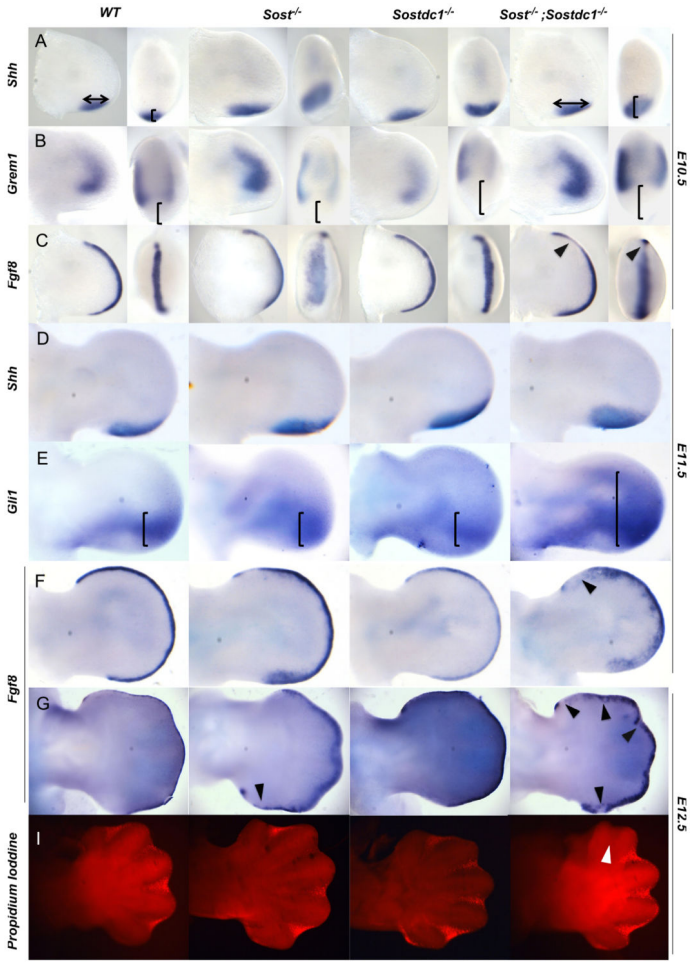

Fig. 6.

Altered SHH and FGF signaling causes polydactyly and syndactyly. *Shh* domain was expanded along the anterior–posterior and proximal–distal axis in *Sost*$^{-/-}$ and *Sost*$^{-/-}$; *Sostdc1*$^{-/-}$ relative to *WT* and *Sostdc1*$^{-/-}$ limb buds at E10.5 (A, arrows, bracket) and E1 1.5 (D). Downstream of *Shh*, *Gli1* expression was dramatically expanded in *Sost*$^{-/-}$; *Sostdc1*$^{-/-}$ E11.5 limb buds relative to all other genotypes (E, brackets). *Grem1* expression was absent in *Shh* positive region, and in *Sostdc1*$^{-/-}$ and *Sost*$^{-/-}$; *Sostdc1*$^{-/-}$ limbs the *Grem1* domain was reduced on the posterior side (B, brackets). *Fgf8* AER expression domain was expanded and disorganized in *Sost*$^{-/-}$ and *Sost*$^{-/-}$; *Sostdc1*$^{-/-}$ limbs, and on the anterior side of the *Sost*$^{-/-}$; *Sostdc1*$^{-/-}$ limbs *Fgf8* expression was reduced in all time points examined (B and F–G, arrows). A reduction in interdigital apoptosis was also detected on the anterior side of *Sost*$^{-/-}$; *Sostdc1*$^{-/-}$ limb buds at E12.5 (I, arrow).

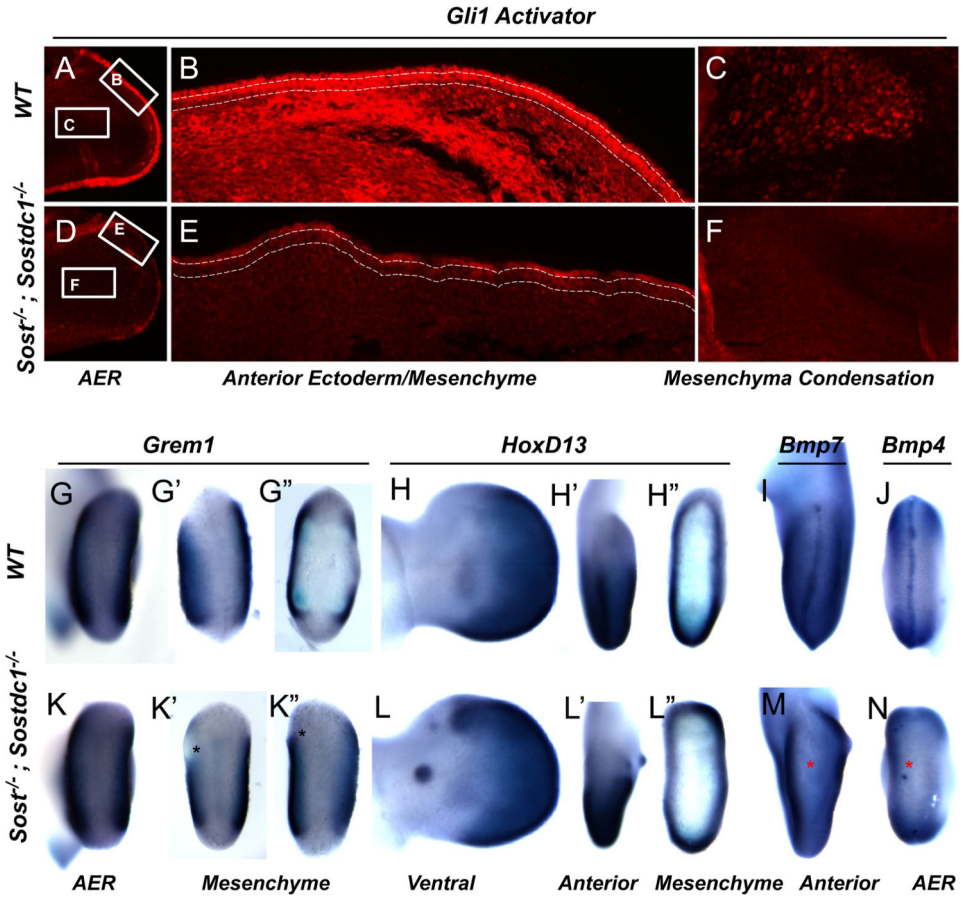

Fig. 7.

Gli3, *Grem1*, *HoxD13*, *Bmp4* and *Bmp7* expression is affected in *Sost*$^{-/-}$; *Sostdc1*$^{-/-}$ E11.5 limbs. Consistent with a reduction in mRNA expression of *Gli3*, *Gli3* activator protein expression was dramatically reduced in the ectoderm of *Sost*$^{-/-}$; *Sostdc1*$^{-/-}$ E11.5 limbs (A and D). Higher magnification images of the anterior region of the limb showed a dramatic reduction in *Gli3* both in the ectoderm (marked by dashed lines) and the underlying mesenchyme (B and E). Similarly, the pre-chondrocytes in the cartilage condensation stained positive for *Gli3* in the *WT* limbs, but had little expression in the double knockouts (F). *Grem1* expression was reduced in the anterior mesenchyme in double knockout (K′–K″) relative to WT limbs (G′–G″). Asterisks indicate region of lost anterior expression. *HoxD13* was ectopically up-regulated in the anterior mesenchyme in the regions corresponding to digit 1 (L, L′, and L″; green arrows) and on the ventral side of the autopod in an ectodermal nubbin (L′ green arrow). Both *Bmp4* and *Bmp7* expression was absent from the AER (M and N; red asterisks). Views are indicated at the bottom of the figure.

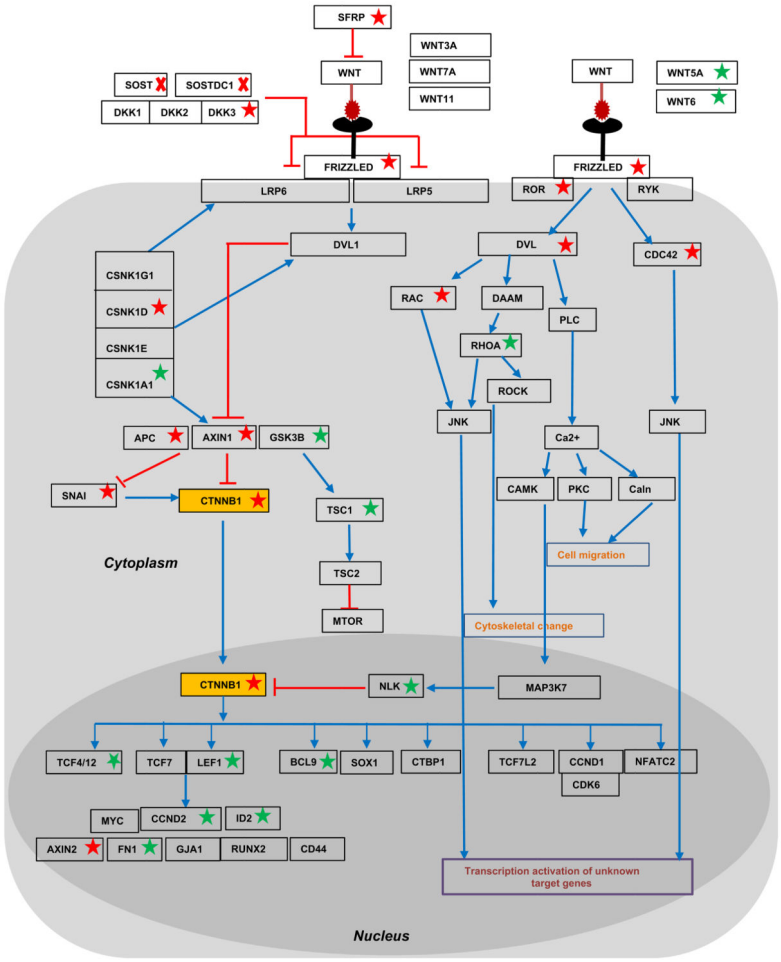

Fig. 8.

Transcriptional changes in the WNT signaling pathway of E11.5 *Sost*$^{-/-}$; *Sostdc1*$^{-/-}$ limbs. Genes found to be transcriptionally up- or down- regulated by more than 2-fold in *Sost*$^{-/-}$;*Sostdc1*$^{-/-}$ limb buds are marked by a green or red star, respectively. Red arrows mark inhibitory relationships, and blue arrows mark other relationships such as transcriptional up-regulation or protein stabilization. β-catenin (CTNNB1) was found to be down-regulated (yellow box).

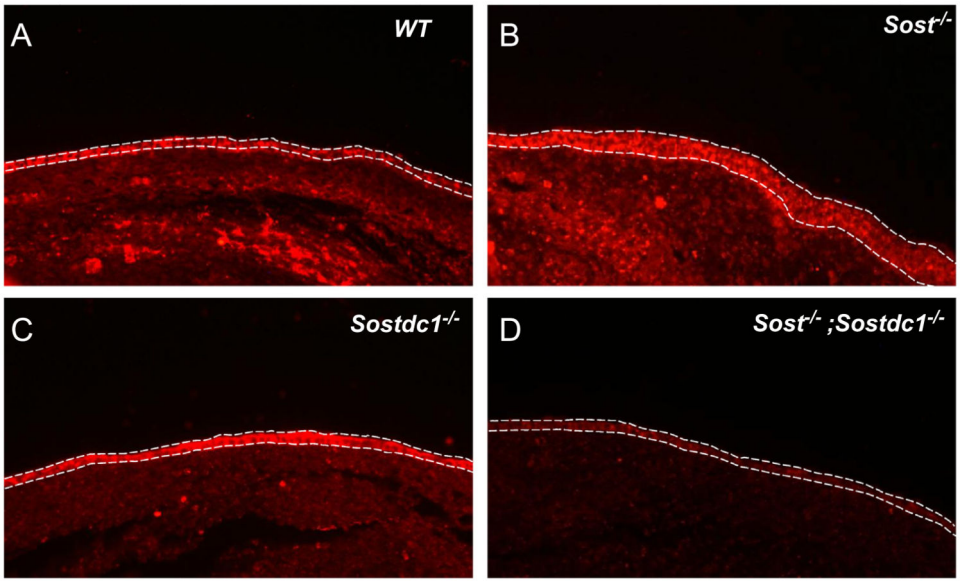

Fig. 9.

Activated β-catenin is dramatically reduced in *Sost*$^{-/-}$; *Sostdc1*$^{-/-}$ limbs. Lack of *Sost* up-regulates WNT signaling as evidenced by increased staining for activated β-catenin in the ectoderm (marked by dashed lines) and underlining mesenchyme (B). *Sost*$^{-/-}$ ectoderm also appears thicker than all other genotypes; lack of *Sostdc1* has little effect on ectodermal β-catenin (C), but causes a slight reduction in the mesenchyme; removing both *Sost* and *Sostdc1* dramatically reduces both ectodermal and mesenchymal activated β-catenin protein (D).

Table 1

Autopod phenotypic analysis of *Sost* and *Sostdc1* single and double knockout mice.

Genotype	Normal	Syndactyly	Ventral pigment	Digit duplication
***Sost*$^{-/-}$**	95	4	1	0
***Sostdc1*$^{-/-}$**	83	0	17	0
***Sost*$^{-/-}$; *Sostdc1*$^{-/-}$**	53	6	10[a]	36[b]

[a] 1 neonate had an extra dermal pad.

[b] 1 neonate had syndactyly; 4 had ventral pigmentation.

Table 2

Differentially expressed genes in the *Sost*; *Sostdc1* KO E11.5 forelimb.

	Up	LogFC	FC	*p*-value	Down	LogFC	FC	*p*-value
WNT signaling	Tcf12	2.52	5.74	0.00020	Sfrp1	−3.06	8.31	0.00024
	Id2	2.48	5.61	0.00008	Dvl2	−2.93	7.61	0.00102
	Fn1	2.41	5.34	0.00671	Fzd1	−2.92	7.57	0.00038
	Gsk3b	2.08	4.22	0.00039	Ror1	−2.66	6.32	0.00230
	Bcl9	1.93	3.82	0.00042	Ctnnb1	−2.40	5.27	0.00015
	Ccnd2	1.85	3.61	0.00512	Snai1	−1.97	3.91	0.00004
	Nlk	1.81	3.51	0.00055	Apc	−1.91	3.75	0.00036
	Lef1	1.72	3.29	0.01267	Frzb	−1.84	3.57	0.00422
	Wnt5a	1.52	2.86	0.01145	Fzd6	−1.83	3.55	0.00022
	Tcf4	1.35	2.56	0.00264	Csnk1d	−1.77	3.40	0.00048
	RhoA	1.33	2.51	0.00155	Axin2	−1.65	3.15	0.00170
	Wnt6	1.16	2.23	0.00010	Cdc42	−1.62	3.07	0.00010
	Csnk1a1	1.06	2.08	0.00400	Fzd7	−1.48	2.79	0.00348
	Tsc1	1.06	2.06	0.00187	Rac1	−1.46	2.75	0.00004
					Axin1	−1.44	2.72	0.00025
					Dkk3	−1.12	2.16	0.00094
BMP signaling					Twsg1	−3.94	15.33	0.00171
					Smad3	−3.66	12.63	0.00022
					Nog	−2.47	5.56	0.00002
					Bmp1	−2.30	4.94	0.00017
					Bmpr1b	−2.05	4.14	0.00388
					Bmp7	−1.40	2.64	0.00101
					Bmp2k	−1.12	2.17	0.00715
					Bmpr2	−1.07	2.09	0.00832
FGF signaling	Fgf8	1.28	2.43	0.00453	Fgfr2	−2.52	5.72	0.00007
					Fgfr1	−2.31	4.95	0.00001
					Fgfr3	−1.51	2.84	0.00469
Homeobox transcription factors	Hoxa10	2.06	4.16	0.00675	Hoxd13	−3.60	12.12	0.00006

	Up	LogFC	FC	*p*-value	Down	LogFC	FC	*p*-value
	Hoxd4	1.93	3.80	0.00014	Tbx15	−3.06	8.38	0.00061
	Hoxc8	1.06	2.08	0.03535	Sox4	−2.96	7.80	0.00230
					Prrx1	−2.64	6.23	0.00080
					Hoxc5	−2.39	5.25	0.00016
					Hoxd12	−2.11	4.33	0.00027
					Sox6	−1.95	3.85	0.00548
					Sox5	−1.50	2.83	0.00700
					Hoxd11	−1.36	2.56	0.00054
					Pitx2	−1.34	2.53	0.028202
					Hoxc6	−1.27	2.42	0.00275
					Sox7	−1.05	2.06	0.00024
SHH signaling	Shh	1.83	3.65	0.03943	Gli3	−1.88	3.68	0.00352
	Ptch1	1.78	3.44	0.00635				
	Gli1	1.20	2.30	0.005846				
TGFβ signaling					Tgfbr1	−4.75	27.03	0.00161
					Smad3	−3.66	12.63	0.00022
					Tgfbr2	−2.13	4.37	0.00108
					Smurf2	−1.67	3.18	0.0001
					Tgfbr3	−1.51	2.84	0.00085
					Acvr1	−1.48	2.79	0.003522
					Smurf1	−1.41	2.66	0.01048
					Tgfb1	−1.02	2.02	0.00096